A Letters Journal Exploring the Frontiers of Physics

September 2022

EPL, **139** (2022) 51001 www.epljournal.org
doi: 10.1209/0295-5075/ac85d6

Non-Arrhenius barrier crossing dynamics of non-equilibrium non-Markovian systems

Laura Lavacchi[a], J. O. Daldrop and Roland R. Netz[b]

Freie Universität Berlin, Fachbereich Physik - 14195 Berlin, Germany

received 19 May 2022; accepted in final form 1 August 2022
published online 11 August 2022

Abstract – The non-equilibrium non-Markovian barrier crossing dynamics of a one-dimensional massive coordinate, described by the non-equilibrium version of the generalized Langevin equation with unequal random and friction relaxation times, is studied by simulations and analytical methods. Within a harmonic approximation, a general formula for the barrier crossing time is derived which agrees favorably with simulations. Non-equilibrium random forces with a relaxation time longer than the friction relaxation time induce non-Arrhenius behavior and dramatically increase the barrier crossing time; within the harmonic theory this corresponds to a reduced effective temperature which also modifies the spatial and velocity distributions.

Biological systems are generally far from equilibrium because mechanical and chemical forces act and produce a net energy flow through the system. The non-equilibrium character gives rise to many salient and not fully understood properties that are studied by novel experimental systems and theoretical models [1–5]. Topics of interest include phase transitions induced by non-equilibrium effects [6–8], violations of the fluctuation-dissipation theorem [9–13], mechanical properties of active gels [14,15] and motility patterns of cells and organisms [16–19].

Of particular interest are non-equilibrium reaction kinetics, *i.e.*, the influence of non-thermal forces on barrier crossing dynamics in some physical or abstract reaction coordinate space, because here the fields of non-equilibrium statistical mechanics, non-Markovian dynamics and rare phenomena meet [20,21]. As examples we mention metastable evolutionary dynamics [22], barrier effects on motion patterns of mammals [23] and cancer cells [24], the effects of active fluctuations on the zipping/unzipping dynamics of RNA hairpins [25], protein folding under non-equilibrium conditions [26] and chemical reactions in the presence of strong time-dependent electric fields [27].

Arrhenius showed that the chemical reaction time under thermal (*i.e.*, equilibrium) conditions, which corresponds to the mean-first-passage time (MFPT) to reach the barrier top of a suitable reaction coordinate, depends exponentially on the barrier free energy height U_0 according to $\tau_{MFP} \sim e^{(U_0/k_BT)}$ [28]. For Markovian systems the pre-exponential factor depends on the effective friction and effective mass [29–31] and satisfactorily describes reaction-diffusion processes [32], chemical reactions [33], protein folding [34–36] and nucleic-acid hairpin formation [37]. All real systems exhibit finite relaxation times, which give rise to memory effects and can sensitively modify the pre-exponential factor [38–44]. Such non-Markovian effects are important for molecular conformational dynamics [45,46], chemical reaction kinetics [47], protein folding [48–51] as well as colloidal dynamics in viscoelastic materials [52]. Note that for equilibrium systems, friction, inertial as well as memory effects only modify the pre-exponential factor, but not the exponential Arrhenius term itself.

We study the barrier crossing dynamics of a one dimensional non-equilibrium non-Markovian model, where the single-exponential relaxation times of the friction memory kernel and the random force are different [18,20,21] and thus the fluctuation-dissipation theorem is broken. This is a rather general model that by projection and dimensional reduction can be derived from a wide class of different microscopic non-equilibrium systems [15,18]. Our analytical calculations show that this particular form of non-equilibrium not only changes the pre-exponential factor but drastically modifies the exponential Arrhenius

[a]E-mail: lauraluna@zedat.fu-berlin.de
[b]E-mail: rnetz@physik.fu-berlin.de (corresponding author)

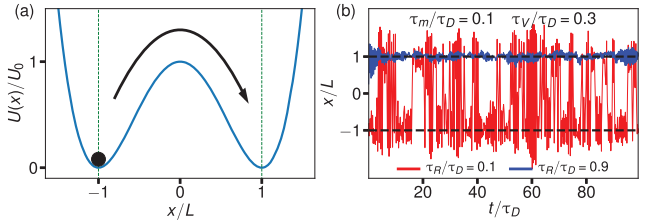

Fig. 1: (a) Schematic barrier crossing of a particle in a double-well potential defined in eq. (3). (b) Non-equilibrium simulation trajectories for moderate barrier height $\beta U_0 = 3$, high friction $\tau_m/\tau_D = 0.1$ and rescaled friction memory time $\tau_V/\tau_D = 0.3$. The red trajectory is for rescaled random correlation time $\tau_R/\tau_D = 0.1$ and shows many barrier crossing events, the blue trajectory for $\tau_R/\tau_D = 0.9$ shows no barrier crossing event.

factor itself. Our derived closed-form expression for the MFPT demonstrates that the modification of the Arrhenius factor can be described by an effective temperature, that is proportional to the square of the friction and random relaxation-time ratio, in good agreement with simulations. The same effective temperature also describes the non-equilibrium position and velocity distributions. In a previous study on non-equilibrium barrier crossing, a similarly defined effective temperature was shown to capture the non-equilibrium modification of the transition-path time [53]. The effect of the random-force correlation time on the barrier crossing dynamics is illustrated by two non-equilibrium simulation trajectories in fig. 1, where the random-force correlation time is shorter (red trajectory) and longer (blue trajectory) than the friction correlation time, with all other parameters being the same: the red trajectory shows many barrier crossing events, while the blue trajectory does not show a single barrier crossing over the same simulation time. From these sample trajectories, we conclude that an increase of the random-force correlation time increases the mean barrier crossing time.

Our model is based on the approximate generalized Langevin equation (GLE) with linear friction

$$m\ddot{x}(t) = -\int_{t_0}^{t} \Gamma_V(t-t')\dot{x}(t')\mathrm{d}t' - \nabla U(x(t)) + F_R(t), \quad (1)$$

where m is the particle mass, $\Gamma_V(t)$ the friction memory kernel, t_0 some initial time and $F_R(t)$ denotes the random force characterized by the general autocorrelation

$$\langle F_R(t)F_R(t')\rangle = \beta^{-1}\Gamma_R(t-t'), \quad (2)$$

where β is a numerical constant. This version of the GLE has been recently shown to follow from an exact form of the GLE in the limit when the correlations between particle velocity and random force are homogeneous in reaction coordinate space and thus corresponds to a physically sound and realizable asymptotic form [54], the main restriction is that non-linear friction effects are neglected. The potential $U(x)$ is time-independent and thus corresponds to the potential of mean force that describes the stationary equilibrium distribution of the reaction coordinate. As a potential that leads to barrier crossing events, we choose a double well

$$U(x) = U_0\left[\left(\frac{x}{L}\right)^2 - 1\right]^2, \quad (3)$$

where $2L$ is the separation between the minima and U_0 is the barrier height.

In equilibrium, the fluctuation-dissipation theorem predicts $\Gamma_R(t) = \Gamma_V(t)$ and $\beta^{-1} = k_BT$ equals the heat bath thermal energy. In the general non-equilibrium scenario, $\Gamma_R(t)$ and $\Gamma_V(t)$ are independent functions, which for simplicity we choose as single exponentials,

$$\Gamma_R(t) = \frac{\gamma_R}{\tau_R}e^{-\frac{|t|}{\tau_R}}, \quad (4)$$

$$\Gamma_V(t) = \frac{\gamma_V}{\tau_V}e^{-\frac{|t|}{\tau_V}}, \qquad \text{for} \quad t > 0, \quad (5)$$

and β does not correspond to the heat-bath temperature. We normalize $\Gamma_R(t)$ and $\Gamma_V(t)$ such that their integral is independent of the memory times, τ_R and τ_V, which allows us to decouple memory time effects from friction effects (note that in a previous treatment of a similar model a different normalization of these memory functions was chosen [53]). With no loss of generality, we consider equal prefactors $\gamma_R = \gamma_V = \gamma$, since different prefactors can be absorbed into the definition of β in eq. (2). For different random and friction memory times, $\tau_R \neq \tau_V$, the fluctuation-dissipation theorem is irrevocably violated and thus the system is out of equilibrium [55–57]. The non-equilibrium version of the GLE in eq. (1) describes non-equilibrium systems in terms of a one-dimensional reaction coordinate that is coupled to a non-thermal random force and subject to a time-independent potential, it can be derived by dimensional reduction of microscopic non-equilibrium models that are coupled to multiple heat baths at different temperatures [15]. Two other time scales characterize the model, namely the inertial time $\tau_m = m/\gamma$ and the diffusion time $\tau_D = L^2\gamma\beta$.

We first present analytical results for the MFPT based on the positional autocorrelation function $C(t) = \langle x(t)x(0)\rangle$. For this we employ a harmonic approximation of eq. (1) and use $U_{\mathrm{har}}(x) = Kx^2/2$, where K is the second derivative of the double-well potential at the minima, $K = U''(L) = 8U_0/L^2$. The calculation we present here significantly generalizes our previous derivation [42], as will be pointed out below. Fourier transforming eq. (1) for $t_0 \to -\infty$ and solving for $\tilde{x}(\omega)$, we obtain

$$\tilde{x}(\omega) = \frac{\tilde{F}_R(\omega)}{K - m\omega^2 + i\omega\tilde{\Gamma}_V^+(\omega)} \equiv \tilde{\chi}(\omega)\tilde{F}_R(\omega), \quad (6)$$

which defines the response function $\tilde{\chi}(\omega)$. The half-sided Fourier transform $\tilde{\Gamma}_V^+(\omega)$ of $\Gamma_V(t)$ is given by

$$\tilde{\Gamma}_V^+ = \int_0^\infty \mathrm{d}t e^{-i\omega t}\Gamma_V(t) = \frac{\gamma}{1 + i\omega\tau_V}, \quad (7)$$

while the Fourier transform of the symmetric random force correlation $\Gamma_R(t)$ is

$$\tilde{\Gamma}_R(\omega) = \tilde{\Gamma}_R^+(\omega) + \tilde{\Gamma}_R^+(-\omega) = \frac{2\gamma}{1+\omega^2\tau_R^2}. \tag{8}$$

The Fourier transform of $C(t)$ is given by $\tilde{C}(\omega) = \beta^{-1}\tilde{\Gamma}_R(\omega)\tilde{\chi}(\omega)\tilde{\chi}(-\omega)$ and reads (see the Supplementary Material `Supplementarymaterial.pdf` (SM))

$$\tilde{C}(\omega) = \frac{2\gamma\beta^{-1}(1+\omega^2\tau_R^2)^{-1}}{\left(K-\omega^2\left[m-\frac{\tau_V\gamma}{1+\tau_V^2\omega^2}\right]\right)^2+\frac{\omega^2\gamma^2}{(1+\omega^2\tau_V^2)^2}}. \tag{9}$$

This can be rewritten in a form that corresponds to the standard result for the memory-less harmonic oscillator in equilibrium (*i.e.*, $\tau_V = \tau_R = 0$),

$$\tilde{C}(\omega) = \frac{2\gamma_{\rm eff}\beta_{\rm eff}^{-1}}{(K-m_{\rm eff}\omega^2)^2+\omega^2\gamma_{\rm eff}^2}, \tag{10}$$

where we have introduced effective frequency-dependent friction, mass and temperature

$$\gamma_{\rm eff} = \frac{\gamma}{1+\tau_V^2\omega^2}, \tag{11a}$$

$$m_{\rm eff} = m - c_1\tau_V\gamma_{\rm eff}, \tag{11b}$$

$$\beta_{\rm eff} = \frac{1+\omega^2\tau_R^2}{1+\omega^2\tau_V^2}\beta. \tag{11c}$$

The mapping introduced here is valid for arbitrary frequencies and for non-equilibrium situations, whereas in our previous work we considered the equilibrium case and the asymptotic limits of high and low frequencies separately [42]. We have introduced a numerical constant that in the harmonic case takes the exact value $c_1 = 1$ and will be used as a fit parameter to account for non-harmonic corrections. For $\tau_R = \tau_V$ equilibrium is recovered and $\beta_{\rm eff} = \beta$, for $\tau_R = \tau_V = 0$ the equilibrium Markovian limit is recovered and additionally $\gamma_{\rm eff} = \gamma$ and $m_{\rm eff} = m$. Note that the potential curvature K is not renormalized. In the overdamped case, characterized by a vanishing bare mass $m = 0$, the effective mass $m_{\rm eff}$ would become negative. Thus, a finite bare mass m is needed in order to regularize the dynamics of the system in our analytical approach. In the low and high friction limits, eq. (10) is dominated by the poles $\omega_L^2 = K/m_{\rm eff}$ for $Km_{\rm eff} > \gamma_{\rm eff}^2$ and $\omega_H^2 = -K^2/\gamma_{\rm eff}^2$ for $Km_{\rm eff} < \gamma_{\rm eff}^2$, respectively (see the SM). From these characteristic frequencies we obtain from eq. (11a) the effective friction in the low and high friction limits (see the SM),

$$\gamma_{\rm eff}^L = \frac{\gamma}{1+c_2\tau_V^2K/m}, \tag{12a}$$

$$\gamma_{\rm eff}^H = \frac{\gamma}{2}\left(1+\sqrt{1+c_3(2K\tau_V/\gamma)^2}\right), \tag{12b}$$

from which the effective mass $m_{\rm eff}$ and the effective temperature $\beta_{\rm eff}$ in the low and high friction limits follow from

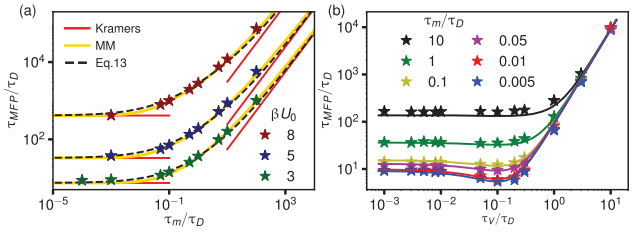

Fig. 2: (a) MFPT in the equilibrium Markovian limit ($\tau_V = \tau_R = 0$) as a function of rescaled mass τ_m/τ_D for three different βU_0. Comparison of simulation results (symbols), eq. (13) (dashed lines) and Melnikov-Meshkov (MM) theory [30] (colored lines). Red straight lines show the Kramers limits [29,58]. (b) MFPT in the equilibrium non-Markovian case ($\tau_V = \tau_R \neq 0$) for $\beta U_0 = 3$ and various τ_m/τ_D as a function of rescaled memory time τ_V/τ_D. Simulation results (symbols) are compared with eq. (14) (lines).

eqs. (11b) and (11c) by insertion. We introduced two more numerical constants c_2 and c_3 that will be used as fit parameters for describing our numerical data.

Using the Markovian mapping in eq. (10), we now construct an expression for the mean-first passage time $\tau_{\rm MFP}$ between the two potential wells at $\pm L$ for the non-Markovian non-equilibrium case. First we consider the equilibrium scenario, defined by $\tau_R = \tau_V$, in which case $\beta_{\rm eff} = \beta$, as follows from eq. (11c), and start with the Markovian limit, $\tau_R = \tau_V = 0$. From the classical Kramers results in the high and low-friction limits, $\tau_{\rm MFP} = e^{\beta U_0}2\sqrt{2}\pi\gamma/K$ and $\tau_{\rm MFP} = e^{\beta U_0}3\pi m/(8\sqrt{2}\beta U_0\gamma)$, respectively [29,58], we construct the heuristic interpolating expression

$$\tau_{\rm MFP} = e^{\beta U_0}\left[\frac{1}{\beta U_0}\frac{3\pi}{8\sqrt{2}}\frac{m}{\gamma} + 2\sqrt{2}\pi\frac{\gamma}{K} + 4\sqrt{2\frac{m}{K}}\right]. \tag{13}$$

Note that we have simply summed the two asymptotic limits and added a crossover term. In fig. 2(a) we compare simulation results for $\tau_{\rm MFP}$ (data points) with the heuristic formula eq. (13) (dashed line) and with Melnikov-Meshkov theory [30] (orange line), the latter becoming exact in the high-barrier limit (see the SM), for three different barrier heights. Details on the simulation methods are given in the SM. The agreement is very good, which means that the numerical simulations are converged and that the heuristic expression eq. (13) works. The Kramers limits are denoted by red lines in fig. 2(a).

We for now stay in equilibrium but consider the more general non-Markovian case and replace the friction coefficient and mass in eq. (13) by their effective expressions in eqs. (11). This only has to be done for the low-friction term proportional to m/γ in eq. (13), because here the resulting effects are dominant compared to the high-friction term proportional to γ/K (or the crossover term) in eq. (13). This is also reflected by the fact that fitting the simulation data for the MFPT with the heuristic formula, we obtain a very small value $c_3 = 0.01$ so that $\gamma_{\rm eff}^H \approx \gamma$

(see the SM). From eqs. (11) and (12) we find in the low-friction limit $m^L_{\rm eff}/\gamma^L_{\rm eff} = m/\gamma - c_1\tau_V + c_2\tau_V^2 K/\gamma$, which shows that memory has two opposing effects: For small τ_V the MFPT eq. (13) goes down due to mass renormalization, thus short memory accelerates barrier crossing, while for long memory the MFPT goes up due to friction renormalization, *i.e.*, long memory slows down barrier crossing [38,40,42]. We also see that the effect memory has on the MFPT survives in the overdamped scenario, $m = 0$, since the memory correction terms are independent of the bare mass. We combine the memory acceleration term with the overdamped contribution in eq. (13) according to $\gamma/K - c_1\tau_V/(\beta U_0) \approx (\gamma/K)/(1 + c_1 K\tau_V/(\gamma\beta U_0))$, which ensures that $\tau_{\rm MFP}$ stays positive and improves the description of the numerical data. We thereby derive the final expression for the MFPT in the equilibrium non-Markovian case, which is equivalent to a previously suggested heuristic formula [42],

$$\tau_{MFP} = e^{\beta U_0}\left[\frac{1}{\beta U_0}\frac{3\pi}{8\sqrt{2}}\left(\frac{m}{\gamma}+\frac{c_2 K\tau_V^2}{\gamma}\right) + \frac{2\sqrt{2}\pi\gamma}{K}\frac{1}{1+3c_1 K\tau_V/(32\beta U_0\gamma)} + 4\sqrt{2\frac{m}{K}}\right]. \quad (14)$$

The harmonic result is recovered for $c_1 = 1 = c_2 = 1$. By fitting to simulation data in fig. 2(b) for fixed barrier height $\beta U_0 = 3$ and a few different rescaled masses τ_m/τ_D (symbols), we obtain $c_1 = 64/3$ and $c_2 = 2/3$, which accounts for the fact that the simulated potential in eq. (3) is not harmonic. We see that the formula eq. (14) is very accurate for general mass/friction ratios and rescaled memory times τ_V/τ_D.

We now turn to the non-equilibrium case $\tau_V \neq \tau_R$. From eq. (11c) and the poles ω_L and ω_H, we obtain

$$\frac{\beta^L_{\rm eff}}{\beta} = \frac{\tau_R^2 + m/K - c_1\tau_V\gamma^L_{\rm eff}/K}{\tau_V^2 + m/K - c_1\tau_V\gamma^L_{\rm eff}/K}, \quad (15)$$

$$\frac{\beta^H_{\rm eff}}{\beta} = \frac{\tau_R^2 - (\gamma^H_{\rm eff}/K)^2}{\tau_V^2 - (\gamma^H_{\rm eff}/K)^2}. \quad (16)$$

In the limits $\tau_m/\tau_V < 1$, $\tau_m/\tau_R < 1$, $\gamma/(K\tau_V) < 1$, $\gamma/(K\tau_R) < 1$, which hold for the simulated systems, as we demonstrate below, we can write

$$\beta_{\rm NEQ}/\beta = \tau_R^2/\tau_V^2 \approx \beta^L_{\rm eff}/\beta \approx \beta^H_{\rm eff}/\beta. \quad (17)$$

We see that the effective temperature $\beta^{-1}_{\rm NEQ}$ depends quadratically on the ratio of the memory friction time τ_V and the random relaxation time τ_R. Replacing β by $\beta_{\rm NEQ}$, we obtain from eq. (14) our final expression for $\tau_{\rm MFP}$ in the non-Markovian non-equilibrium case,

$$\tau_{\rm MFP} = e^{\beta_{\rm NEQ}U_0}\left[\frac{1}{\beta_{\rm NEQ}U_0}\frac{3\pi}{8\sqrt{2}}\left(\frac{m}{\gamma}+\frac{c_2 K\tau_V^2}{\gamma}\right) + \frac{2\sqrt{2}\pi\gamma}{K}\frac{1}{1+3c_1 K\tau_V/(32\beta_{\rm NEQ}U_0\gamma)} + 4\sqrt{2\frac{m}{K}}\right]. \quad (18)$$

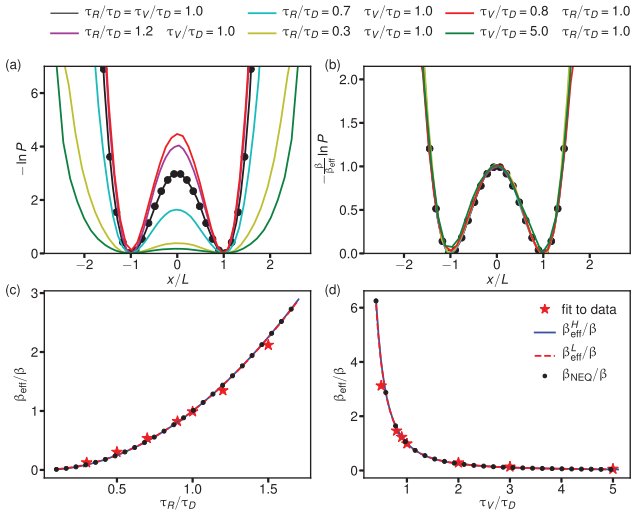

Fig. 3: (a) Logarithmic position distributions for $\tau_m/\tau_D = 0.1$, $\beta U_0 = 3$ and various τ_R/τ_D and τ_V/τ_D. (b) Logarithmic position distributions rescaled by fitting factors $\beta/\beta_{\rm eff}$. In (c) and (d) $\beta_{\rm eff}/\beta$ from fits in (b) (red stars) is compared with the predictions from eqs. (15), (16), (17).

Before comparing eq. (18) with simulation results for $\tau_{\rm MFP}$, we consider the joint position-velocity distribution, which, according to our mapping, is predicted as

$$P(x,v) \propto e^{-\beta_{\rm eff}U(x) - \beta_{\rm eff}v^2 m/2}. \quad (19)$$

Note that we assume the mass prefactor of the kinetic energy not to be renormalized. From this point on, we focus on the overdamped case and choose $\tau_m/\tau_D = 0.1$, because this is the most relevant regime for biophysical applications. In fig. 3(a) we show logarithmic positional distributions $-\ln P(x)$ for various values of τ_V/τ_D and τ_R/τ_D, shifted vertically so that they agree for $x = \pm L$. The simulation data for the equilibrium case $\tau_R = \tau_V$ is denoted by a black line and agrees perfectly with the expected Boltzmann distribution $-\ln P(x) = \beta U(x)$, denoted by black spheres; the non-equilibrium simulation results are shown as colored lines. In fig. 3(b) we show $-(\beta/\beta_{\rm eff})\ln P(x)$ with the prefactor $\beta/\beta_{\rm eff}$ fitted such that the data superimpose. We see that all distributions agree perfectly, meaning that an effective temperature describes the non-equilibrium position distributions well. In figs. 3(c) and (d) we plot the fit results for $\beta_{\rm eff}/\beta$ (red stars) as a function of τ_R/τ_D and τ_V/τ_D, respectively, and obtain perfect agreement with the predictions in eqs. (15), (16), (17). This in particular means that the asymptotic expression for $\beta_{\rm NEQ}$ in eq. (17) is accurate for the employed parameters.

In fig. 4(a) we show the logarithmic velocity distributions $-\ln P(v)$ for various values of τ_V/τ_D and τ_R/τ_D, shifted vertically so that they agree for $v = 0$. Again, the simulation data for the equilibrium case $\tau_R = \tau_V$ is denoted by a black line and agrees perfectly with the expected Maxwell-Boltzmann distribution

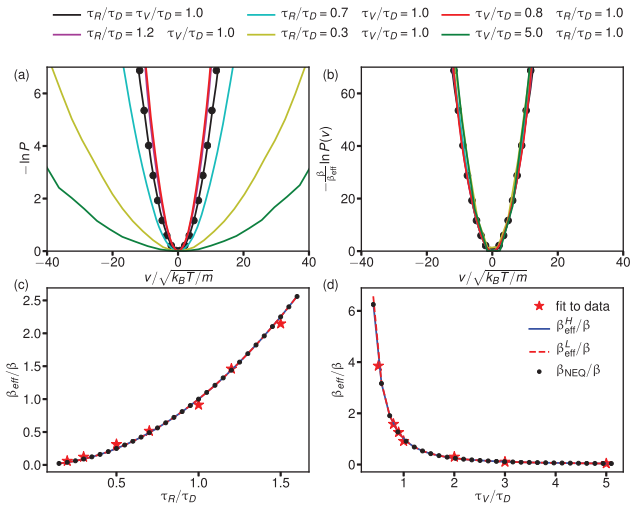

Fig. 4: (a) Logarithmic velocity distributions for $\tau_m/\tau_D = 0.1$, $\beta U_0 = 3$ and various τ_R/τ_D and τ_V/τ_D. (b) Logarithmic velocity distributions rescaled by fitting factors $\beta/\beta_{\rm eff}$. In (c) and (d) $\beta_{\rm eff}/\beta$ from fits in (b) (red stars) is compared with the predictions from eqs. (15), (16), (17) (lines).

$-\ln P(v) = \beta m v^2/2$ (black spheres), the non-equilibrium simulation results are shown as colored lines. In fig. 4(b) we show $-(\beta/\beta_{\rm eff})\ln P(v)$ with fitted prefactors $\beta/\beta_{\rm eff}$ and again find the data to perfectly superimpose. In figs. 4(c) and (d) we favorably compare the fit results for $\beta_{\rm eff}/\beta$ (red stars) with the predictions in eqs. (15), (16), (17). In essence, the position and velocity distributions from our non-equilibrium simulations are perfectly described by an effective temperature that depends on the ratio of memory and random relaxation times according to eq. (17).

Finally, in fig. 5 we compare $\tau_{\rm MFP}$ from simulations (symbols) with eq. (18) as a function of τ_R/τ_V for three different values of τ_V/τ_D, note that equilibrium is recovered for $\tau_R/\tau_V = 1$. We see that as the ratio τ_R/τ_V increases, $\tau_{\rm MFP}$ grows dramatically (note the logarithmic vertical scale), which reflects the decrease of the effective temperature in eq. (17) and the divergence of the exponential Arrhenius factor in eq. (18). In contrast, for decreasing ratio τ_R/τ_V the MFPT levels off, which reflects a competition of the pre-exponential memory slow-down factor proportional to τ_V^2 with the exponential factor in eq. (18).

In conclusion, by solving the non-equilibrium non-Markovian harmonic oscillator in terms of its effective friction, mass and temperature, and using the Kramers results for the Markovian barrier crossing dynamics, we analytically derive a closed-form expression for the non-equilibrium non-Markovian barrier crossing dynamics in a double well that holds in the low and high friction regimes. Our derived expression for the MFPT agrees with a previously suggested heuristic formula for the MFPT in the non-Markovian equilibrium limit [42,43] and describes our non-equilibrium simulation results rather well without additional fitting parameters. Whereas memory and

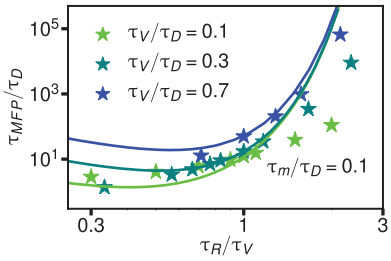

Fig. 5: Non-equilibrium MFPT as a function of the relaxation-time ratio τ_R/τ_V for various values of τ_V/τ_D for fixed $\beta U_0 = 3$ and $\tau_m/\tau_D = 0.1$. The lines show the predictions from eq. (18) and the stars denote simulation data.

inertial effects only influence the exponential prefactor of the MFPT, non-equilibrium effects modify the exponential Arrhenius factor itself and thus drastically modify barrier crossing times. The random correlation time τ_R and the memory friction time τ_V influence the non-equilibrium MFPT in a markedly asymmetric fashion, the MFPT increases steeply for $\tau_R/\tau_V > 1$ but rather levels off for $\tau_R/\tau_V < 1$. These findings are possibly relevant for *in vivo* non-equilibrium protein folding, since in recent experiments on the folding speed of a nascent polypeptide during translation a delay of the folding has been measured [26]. Whether co-translational folding is characterized by increased random-force relaxation times seems plausible but of course has to be substantiated by microscopic modeling. We note that our derived result for the MFPT depends crucially on the form of our friction and random-force memory functions, who are taken as single-exponential functions and whose integrals are defined to be independent of the memory times. In passing we note that our analytically derived effective temperature also describes position and velocity distribution of our non-linear barrier crossing system very accurately even far away from equilibrium.

* * *

We acknowledge support by Deutsche Forschungsgemeinschaft, Grant CRC 1114, code 235221301, Project B03 and by the European Research Council Advanced Grant NoMaMemo Grant 835117.

Data availability statement: All data that support the findings of this study are included within the article (and any supplementary files).

REFERENCES

[1] Dzubiella J., Hoffmann G. P. and Löwen H., *Phys. Rev. E*, **65** (2002) 021402.
[2] Ramaswamy S., *Annu. Rev. Condens. Matter Phys.*, **1** (2010) 323.
[3] Bechinger C., Di Leonardo R., Löwen H., Reichhardt C., Volpe G. and Volpe G., *Rev. Mod. Phys.*, **88** (2016) 045006.

[4] Ginot F., Theurkauff I., Levis D., Ybert C., Bocquet L., Berthier L. and Cottin-Bizonne C., *Phys. Rev. X*, **5** (2015) 011004.
[5] Fang X., Kruse K., Lu T. and Wang J., *Rev. Mod. Phys.*, **91** (2019) 045004.
[6] Jäger S., Schmidle H. and Klapp S. H. L., *Phys. Rev. E*, **86** (2012) 011402.
[7] Grosberg A. Y. and Joanny J.-F., *Phys. Rev. E*, **92** (2015) 032118.
[8] Fodor É. and Marchetti M. C., *Physica A*, **504** (2018) 106.
[9] Bohec P., Gallet F., Maes C., Safaverdi S., Visco P. and van Wijland F., *EPL*, **102** (2013) 50005.
[10] Prost J., Joanny J.-F. and Parrondo J. M. R., *Phys. Rev. Lett.*, **103** (2009) 090601.
[11] Dinis L., Martin P., Barral J., Prost J. and Joanny J.-F., *Phys. Rev. Lett.*, **109** (2012) 160602.
[12] Willareth L., Sokolov I. M., Roichman Y. and Lindner B., *EPL*, **118** (2017) 20001.
[13] Netz R. R., *Phys. Rev. E*, **101** (2020) 022120.
[14] Mizuno D., Tardin C., Schmidt C. F. and MacKintosh F. C., *Science*, **315** (2007) 370.
[15] Netz R. R., *J. Chem. Phys.*, **148** (2018) 185101.
[16] Helbing D., *Rev. Mod. Phys.*, **73** (2001) 1067.
[17] Dieterich P., Klages R., Preuss R. and Schwab A., *Proc. Natl. Acad. Sci. U.S.A.*, **105** (2008) 459.
[18] Mitterwallner B. G., Schreiber C., Daldrop J. O., Rädler J. O. and Netz R. R., *Phys. Rev. E*, **101** (2020) 032408.
[19] Selmeczi D., Li L., Pedersen L. I. I., Nrrelykke S. F., Hagedorn P. H., Mosler S., Larsen N. B., Cox E. C. and Flyvbjerg H., *Eur. Phys. J. ST*, **157** (2008) 1
[20] Banik S. K., Chaudhuri J. R. and Ray D. S., *J. Chem. Phys.*, **112** (2000) 8330.
[21] Cherayil B. J., *J. Chem. Phys.*, **155** (2021) 244903.
[22] Van Nimwegen E. and Crutchfield J. P., *Bull. Math. Biol.*, **62** (2000) 799.
[23] Rico A., Kindlmann P. and Sedláček F., *Folia Zool.*, **56** (2007) 1.
[24] Brückner D. B., Fink A., Rädler J. O. and Broedersz C. P., *J. R. Soc. Interface*, **17** (2020) 20190689.
[25] Vandebroek H. and Vanderzande C., *Soft Matter*, **13** (2017) 2181.
[26] Alexander L. M., Goldman D. H., Wee L. M. and Bustamante C., *Nat. Commun.*, **10** (2019) 2709.
[27] Stensitzki T., Yang Y., Kozich V., Ahmed A. A., Kössl F., Kühn O. and Heyne K., *Nat. Chem.*, **10** (2018) 126.
[28] Arrhenius S., *Z. Phys. Chem.*, **4** (1889) 226.
[29] Kramers H., *Physica*, **7** (1940) 284.
[30] Mel'nikov V. I. and Meshkov S. V., *J. Chem. Phys.*, **85** (1986) 1018.
[31] Best R. B. and Hummer G., *Phys. Rev. Lett.*, **96** (2006) 228104.
[32] Northrup S. H. and Hynes J. T., *J. Chem. Phys.*, **69** (1978) 5246.
[33] Barcilon V., Chen D., R. S. Eisenberg *et al.*, *J. Chem. Phys.*, **98** (1993) 1193.
[34] Chung H. S. and Eaton W. A., *Nature*, **502** (2013) 685.
[35] Chung H. S., Piana-Agostinetti S., Shaw D. E. and Eaton W. A., *Science*, **349** (2015) 1504.
[36] Neupane K., Manuel A. P. and Woodside M. T., *Nat. Phys.*, **12** (2016) 700.
[37] Pyo A. G. T., Hoffer N. Q., Neupane K. and Woodside M. T., *J. Chem. Phys.*, **149** (2018) 115101.
[38] Grote R. F. and Hynes J. T., *J. Chem. Phys.*, **73** (1980) 2715.
[39] Carmeli B. and Nitzan A., *Phys. Rev. Lett.*, **49** (1982) 423.
[40] Pollak E., Grabert H. and Hänggi P., *J. Chem. Phys.*, **91** (1989) 4073.
[41] Berezhkovskii A. and Szabo A., *J. Chem. Phys.*, **122** (2005) 014503.
[42] Kappler J., Daldrop J. O., Brünig F. N., Boehle M. D. and Netz R. R., *J. Chem. Phys.*, **148** (2018) 014903.
[43] Kappler J., Hinrichsen V. B. and Netz R. R., *Eur. Phys. J. E*, **42** (2019) 119.
[44] Lavacchi L., Kappler J. and Netz R. R., *EPL*, **131** (2020) 40004.
[45] Rosenberg R. O., Berne B. J. and Chandler D., *Chem. Phys. Lett.*, **75** (1980) 162.
[46] Daldrop J. O., Kappler J., Brünig F. N. and Netz R. R., *Proc. Natl. Acad. Sci. U.S.A.*, **115** (2018) 5169.
[47] Chaudhury S., Chatterjee D. and Cherayil B. J., *J. Chem. Phys.*, **129** (2008) 075104.
[48] Plotkin S. S. and Wolynes P. G., *Phys. Rev. Lett.*, **80** (1998) 5015.
[49] Das A. and Makarov D. E., *J. Phys. Chem. B*, **122** (2018) 9049.
[50] Singh V. and Biswas P., *J. Stat. Mech.*, **2021** (2021) 063502.
[51] Ayaz C., Tepper L., Brünig F. N., Kappler J., Daldrop J. O. and Netz R. R., *Proc. Natl. Acad. Sci. U.S.A.*, **118** (2021) e2023856118.
[52] Ferrer B. R., Gomez-Solano J. R. and Arzola A. V., *Phys. Rev. Lett.*, **126** (2021) 108001.
[53] Carlon E., Orland H., Sakaue T. and Vanderzande C., *J. Phys. Chem. B*, **122** (2018) 11186.
[54] Ayaz C., Scalfi L., Dalton B. A. and Netz R. R., *Phys. Rev. E*, **105** (2022) 054138.
[55] Baiesi M. and Maes C., *New J. Phys.*, **15** (2013) 013004.
[56] Maes C., Safaverdi S., Visco P., van Wijland F., *Phys. Rev. E*, **87** (2013) 022125.
[57] Puglisi A., Sarracino A. and Vulpiani A., *Phys. Rep.*, **709** (2017) 1.
[58] Kalmykov Y. P., Coffey W. T. and Titov S. V., *J. Chem. Phys.*, **124** (2006) 024107.